Stress and temperature dependence of screw dislocation mobility in α-Fe by molecular dynamics

M. R. Gilbert,[1] S. Queyreau,[2] and J. Marian[2,*]

[1]*EURATOM/CCFE Fusion Association, Culham Science Centre, Abingdon OX14 3DB, United Kingdom*

[2]*Lawrence Livermore National Laboratory, P. O. Box 808, Livermore, California 94551, USA*

(Received 18 June 2011; revised manuscript received 20 September 2011; published 7 November 2011)

The low-temperature plastic yield of α-Fe single crystals is known to display a strong temperature dependence and to be controlled by the thermally activated motion of screw dislocations. In this paper, we present molecular dynamics simulations of $\frac{1}{2}\langle 111\rangle\{112\}$ screw dislocation motion as a function of temperature and stress in order to extract mobility relations that describe the general dynamic behavior of screw dislocations in pure α-Fe. We find two dynamic regimes in the stress-velocity space governed by different mechanisms of motion. Consistent with experimental evidence, at low stresses and temperatures, the dislocations move by thermally activated nucleation and propagation of kink pairs. Then, at a critical stress, a temperature-dependent transition to a viscous linear regime is observed. Critical output from the simulations, such as threshold stresses and the stress dependence of the kink activation energy, are compared to experimental data and other atomistic works with generally very good agreement. Contrary to some experimental interpretations, we find that glide on {112} planes is only apparent, as slip always occurs by elementary kink-pair nucleation/propagation events on {110} planes. Additionally, a dislocation core transformation from compact to dissociated has been identified above room temperature, although its impact on the general mobility is seen to be limited. This and other observations expose the limitations of inferring or presuming dynamic behavior on the basis of only static calculations. We discuss the relevance and applicability of our results and provide a closed-form functional mobility law suitable for mesoscale computational techniques.

DOI: 10.1103/PhysRevB.84.174103 PACS number(s): 61.72.Ff, 61.72.Hh, 07.05.Tp, 28.41.Ak

I. INTRODUCTION

The low-temperature yield behavior of α-Fe single crystals has been well characterized over the years in numerous experimental works.[1–4] Tensile tests in high-purity specimens reveal a strong temperature dependence of the strain rate and flow stress behavior.[5,6] This is known to be a consequence of the thermally activated nature of $\frac{1}{2}\langle 111\rangle$screw dislocation motion in body-centered-cubic (bcc) metals. Because lattice friction in such crystals is typically quite high, at moderate to low stresses, plastic flow can be reduced to the individual motion of screw dislocations, which are known to display much lower mobilities than nonscrew segments. Consequently, by studying single screw dislocation properties and mobilities, many useful insights can be gained into the plastic behavior of Fe and other bcc crystals.

However, experimental measurements concerning single dislocation properties are exceedingly difficult, and only recently have experimental techniques reached a level of resolution capable of isolating individual dislocation behavior,[7,8] such as in bcc Fe.[9] Consequently, a wealth of atomistic simulation studies have been performed over the last decade or so in an attempt to shed light on dislocation structure and core properties and energetics.[10–14] In particular, the stress dependence of the kink-pair (KP) nucleation enthalpy has been the subject of much study.[15–18] Nevertheless, despite these and other significant advances in our understanding of $\frac{1}{2}\langle 111\rangle$screw dislocation properties at the atomistic level, their true impact on plasticity on a more global scale can only be assessed by way of models operating at the mesoscale, e.g., dislocation dynamics or phase fields. Indeed, screw-dislocation-controlled plasticity in α-Fe has been the subject of several dislocation dynamics (DD) works.[19,20] The fundamental input to DD simulations is the so-called mobility function,[21–23] which couples forces acting on dislocation segments to their velocity response. On a more simplistic level, the mobility function relates applied stresses to dislocation velocities, and may be a function of several factors, including temperature, pressure, dislocation character, and internal microstructure.

When measuring dislocation velocities directly from experimental observations, it is typically very difficult to subtract out the effect of the surrounding dislocation environment (impurities, "forest" dislocations, pile-ups, etc.), although notable exceptions exist.[9] Conversely, if used carefully, atomistic simulations can be invaluable in providing dislocation mobility behavior under well-controlled conditions.[24,25] In this paper, we present a molecular dynamics (MD) study of $\frac{1}{2}\langle 111\rangle$screw dislocation motion in bcc Fe as a function of stress and temperature. We then use the MD results to fit analytical functions that describe single dislocation mobility within mesoscale techniques. The main goal of this work is thus to produce MD-fitted mobility laws that can be used to study plastic behavior on longer time and space scales by utilizing methods that transcend the atomistic limit.

At low temperatures and strain rates, screw dislocations are known to move as straight lines, which suggests that only one KP exists at a given time. This is the basis of the so-called *smooth* glide identified in Ref. 26. Such a regime is then governed by KP nucleation, as kink motion proceeds at comparatively high speeds. As the temperature and/or strain rate increase, kink nucleation and propagation can be of the same order of magnitude, leading to rough dislocation lines and, under certain conditions, production of debris. This rough behavior is also observed as the stress approaches the Peierls stress, and is the prelude to the famed phonon drag regime that sets in when kink nucleation is no longer the rate-limiting step.

This paper is organized as follows. First, we optimize the supercell geometry on the basis of the physical process governing each dimension. Second, we perform MD simulations of screw dislocation motion as a function of stress and temperature, and provide the theoretical framework to justify the fitting functions used to produce analytical mobility laws. This is followed by an analysis of the proposed mobilities and the implications for crystal plasticity. Our calculations were performed with the parallel MD code LAMMPS[27] using the EAM potential for Fe developed by Mendelev *et al.*[28] The literature on screw dislocation core properties,[13,14,29,30] Peierls energy and stress,[14,31] and kink structure and formation energies,[17,18,30,31] to name but a few, using this potential is quite abundant, and here we simply note that this potential yields the symmetric core structure (at 0 K) predicted by electronic structure calculations.[13,14,32]

II. METHODOLOGY

Dislocation mobility calculations require long simulation times to allow for a steady state to be reached under each set of conditions. This means that setups such as those employed by Domain and Monnet[13] or Chaussidon *et al.*,[30] which result in finite dimensions along the glide direction (referred to by the authors as "free boundaries"), cannot be used here. Instead, we use periodic boundary conditions along the dislocation line and glide directions, and traction boundaries along the glide-plane normal direction. This imposes certain restrictions on the computational box dimensions L_x (glide direction), L_y (line direction), and L_z (plane normal direction), with each one governed by a specific physical process. Next, we discuss the criteria chosen for the design of each dimension of the supercell on the basis of the relevant physical phenomena.

A. Line direction L_y

At low temperatures and stresses, $\frac{1}{2}\langle 111\rangle$screw dislocations move by nucleation/propagation of kink pairs. These KPs display a stress- and temperature-dependent characteristic separation length that must be contained entirely within the dislocation line. Marian *et al.*[26] showed that short dislocation segments result in two-dimensional (2D) dynamics, which are not representative of dislocation motion at low T. In addition, recent work by Ventelon *et al.*[17] suggests that single kinks in Fe have widths of the order of $w_K = 20b$ in the $\langle 111\rangle$ direction at 0 K. Despite the fact that the calculations by Ventelon *et al.* concern only single, isolated kinks, and thus neglect the interaction between the two kinks of a KP, here we use a lower bound length of $40b$ for our screw dislocation lines, where $b = a_0\frac{\sqrt{3}}{2} \approx 0.25$ nm is the Burgers vector and $a_0 = 0.27$ nm is the lattice parameter for bcc Fe. An upper bound is obtained by striving for the conditions under which the KP mechanism results in linear, smooth glide as defined in Ref. 26 (also termed the "single kink-pair" regime by Chaussidon *et al.*).[30]

As shown there, when the dislocation line is too long, the simulation limitations inherent to MD result in multiple kinks on multiple glide planes, leading to cross kinks. This so-called *rough* regime results in self-pinning and is not representative of plasticity at moderate to low stresses and temperatures. Following the arguments provided by Marian *et al.*,[26] ensuring that only one KP occurs simultaneously requires that the dislocation line length be of the same order as the kink mean free path. An upper limit for L_y is then

$$L_y \approx 2w_K + s_K + X,$$

where s_K is the stable kink span (calculated, e.g., by Ngan and Wen),[33] and X is the kink free path. The most restrictive scenario is that at low stresses (and temperatures), where s_K is highest. On the basis of the work by Ngan and Wen, we take $s_K \approx 20b$. Regarding X, the theory relating it to stress and temperature is well known (cf. Sec. III C), and could be used to calculate it explicitly. However, we have performed preliminary tests in the temperature and stress ranges of interest in this work and have obtained values of $X \approx 20b$ to be satisfactory for our purposes. Hence, we fix $L_y = 80b \approx 19.8$ nm as our dislocation line length in all the simulations.

B. Plane normal direction L_z

In the conventional picture of α-Fe plasticity, supported by numerous experimental studies (cf. Sec. I), slip takes place on {110} planes when they are the most highly stressed planes, regardless of temperature. However, for the potential employed here, this maximum-resolved shear stress (MRSS) plane is also the glide plane only in a narrow range of (low) temperature and stress. Indeed, Domain and Monnet[13] and Chaussidon *et al.*[30] have shown that consistent {110} slip is only attainable under dynamic conditions when free boundaries are used along the glide direction. As pointed out above, these boundary conditions are not suitable for the type of dislocation mobility calculations that we are concerned with here. As the applied stress and simulation temperature increase, screw dislocations are seen to deviate from {110} planes and rotate to glide planes that approach {112}. MD simulations have confirmed that despite gliding on *effective* {112} planes, slip proceeds as a succession of elementary kink nucleation episodes on non-MRSS {110} planes.[26,30]

Therefore, here we have chosen to study dislocation motion on {112} planes, with stress applied to a skin layer consisting of three atomic planes at the top and bottom of the simulation box. These layers are made rigid with respect to the displacement introduced by a screw dislocation, i.e., along the y direction. In this fashion, repulsive forces are generated,[34] resulting in stable glide conditions. Temperature control is also only applied to atoms in the skin region via a Langevin thermostat. Once the dislocated crystallites have been equilibrated at the desired temperature, stress-controlled simulations are performed without any kind of temperature control.

The length of the $\langle 112\rangle$ direction is obtained on the basis of the following arguments:

(i) When stress is initially applied, a shear-stress wave traveling at the speed of sound is generated at each of the skin layers. These waves reach the dislocation and accelerate it before continuing their propagation through the computational box. When they reach the sample limits, they reflect off of the opposite boundaries with inverted sign, which cancels the effect of fresh stress waves coming from the surface. This makes the dislocation stop until these elastic waves reverberate again at the original boundary and restore their sign. This

process repeats itself until the waves are suppressed by viscous damping and scattering (there are ways to mitigated this, e.g., by introducing a stress ramp, rather than a step). As we shall see (e.g., cf. Fig. 3), this results in a transient period during which dislocation mobility is highly scale dependent. With L_z too large, the period of the wave reflections lengthens, extending this transient in time longer than desirable, which could then cause the movement of dislocations to be too intermittent for a steady state to be reached within reasonable MD time scales.

(ii) As we have indicated above, the rigid boundaries where the stress is applied create repulsive forces on the dislocation that stabilize it on the glide plane corresponding to the center of the box. However, because the presumed mechanism of motion on MRSS {112} glide planes is still by complementary KP nucleations on the {110} planes bordering at $\pm 30^\circ$, the image forces must be sufficiently small to not interfere with this natural mechanism. This suggests a z dimension as large as possible.

On the basis of these considerations, a reasonable size was found to be $L_z = 84\sqrt{6}a_0 = 58.7$ nm. Stress was always applied so as to create a Peach-Köhler force in the twinning sense.

C. Glide direction L_x

The physical consideration to keep in mind when designing the dimension L_x along the periodic glide direction $\langle 110 \rangle$ is local heating after each dislocation passage. Fast-moving dislocations leave a "hot" trail in their wake in the regime governed by viscous drag. In contrast to dislocations moving in an *effective* infinite medium, which see only a "fresh" crystal ahead, in MD simulations the dislocation reenters the box after each passage (we emphasize again that single-passage simulations are not acceptable for our dynamic mobility simulations). The residual heat remaining locally on the glide plane dissipates at a given rate that depends on temperature and dissipation direction. If the dislocation encounters a hot glide plane after each passage, the resulting velocity would not be representative of the simulation temperature, and, thus, the computational box must be sufficiently large in the glide direction to ensure that the dislocation travels through a thermalized glide plane during every passage.

To obtain a first-order estimate of L_x, we set up a small $10 \times 10 \times 10a_0$ box with a skin region kept at a constant temperature of 100 K and a central region of atoms initialized at temperatures greater than that value. We then calculate the temperature-decay profile of the central region and fit it to the inverse exponential solution to Newton's law of cooling:

$$T(t) = T_\infty + b_0 \exp(-b_1 t),$$

where, in the simulations, T_∞ is the final target temperature, and b_0 and b_1 are fitting constants that represent, respectively, the initial temperature difference between the central atoms and the skin region at T^∞, and the decay constant. We are particularly interested in the latter, as it gives an idea of the heat-evacuation rate from atoms that are not subjected to temperature control. For the tests performed in Fig. 1 with $T^\infty = 100$ K, we obtain an average value of $b_1 \approx 0.55$ ps^{-1}, corresponding to a time constant of 1.8 ps. As the figure shows, at $t \approx 7$ ps, all of the curves have decayed to the temperature of the heat bath. Then, assuming a maximum dislocation velocity equal to the shear wave velocity of $\approx$3400 m s^{-1} in Fe,[28] the minimum box size along the glide direction is approximately 24 nm. Therefore, we choose a box with $L_x = 60\sqrt{2}a_0 = 24.3$ nm. Before performing dislocation mobility simulations under applied stress, the box is equilibrated at the desired temperature during 20 ps using a Langevin thermostat. After applying stress, the total box temperature was never seen to increase more than 10% above the temperature of the heat bath.

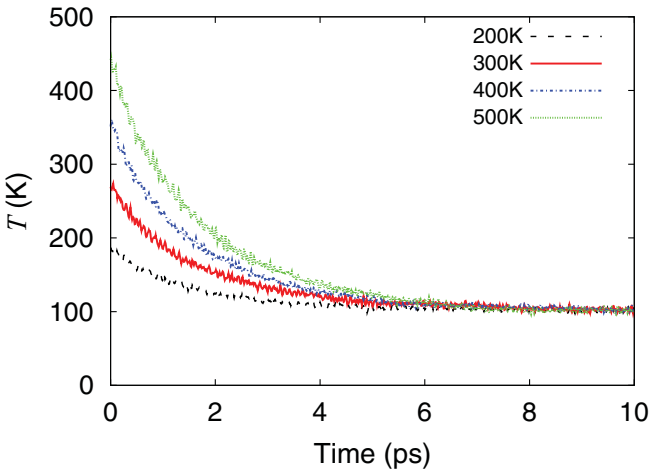

FIG. 1. (Color online) Evolution of the initial temperature in a computational cell after connecting the skin region to a heat reservoir at 100 K. For all the initial temperatures, a decay time constant of $\approx$7 ps is found.

Thus, to summarize this section, we have designed an orthogonal computational box with axes $z \equiv [1\bar{1}2]$, $y \equiv \frac{1}{2}[111]$, and $x \equiv [\bar{1}10]$, corresponding to the line, plane normal, and glide directions, respectively, with dimensions $L_z = 19.9$ nm ($80b$), $L_y = 24.3$ nm, and $L_x = 58.7$ nm. This configuration contains in excess of 2.4 million atoms, which results in nominal strain rates of $1.7 \times 10^{6\sim7}$ s^{-1} for velocities between 10 and 100 m s^{-1}. Figure 2 shows a schematic diagram of the computational box employed.

The simulations were run on massively parallel platforms (>500 processors) at Virginia Tech and Lawrence Livermore National Laboratory. The approximate computational cost of the simulations was 3.5×10^{-5} seconds per time step per atom.

III. RESULTS

A. Raw MD data

The simulations are run for sufficiently long times to overcome the transients discussed previously and develop statistically meaningful behavior. Configuration data were extracted every picosecond, regardless of the applied stress and the temperature. For each configuration, the dislocation core was identified using the centrosymmetry deviation parameter analysis employed in many other studies. From the position of the core, velocities are extracted as the derivative of the displacement-time curves for each case. The processed output of the simulations at 300 K is shown in Fig. 3. Results for all of the other temperatures are qualitatively identical. At each

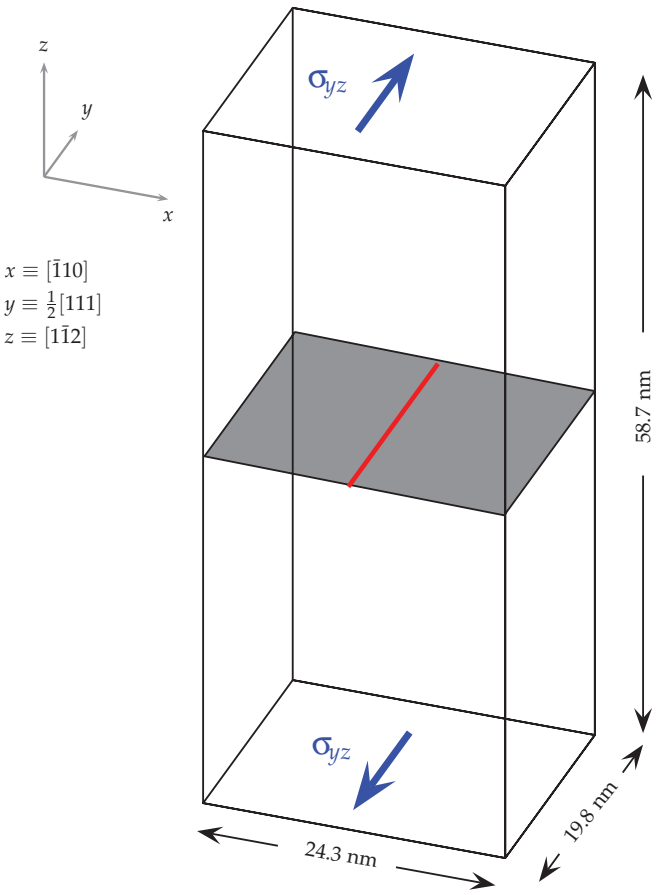

FIG. 2. (Color online) The simulation setup used to measure the velocity response of a $\frac{1}{2}\langle 111\rangle$ screw dislocation to applied stress at finite temperature. The red line represents the dislocation; the shaded plane corresponds to the dislocation glide plane.

temperature, the stress is applied in roughly 50 MPa intervals from zero to the point of "shear melting." This phenomenon occurs when the screw dislocation moves too fast for the local heat generated on the glide plane to dissipate (despite our efforts). Under such conditions, successive reentries through the periodic boundary heat the atomic layers around the glide plane above the melting point of the crystal. This causes the material to literally flow along the glide plane, locally removing any notion of crystallinity and dislocation structure. This is the case for the black curve in Fig. 3, corresponding to an applied stress of 1150 MPa. In addition, the threshold stress for dislocation motion within MD time scales, which we term σ_0, is measured (194 MPa in Fig. 3 for the 300 K case). σ_0 is defined as the stress at which the dislocation moves within the first 100 ps, and is therefore an upper bound on the true threshold stress, imposed by the short MD time scales.

The velocities are measured from the slope of linear fits to the displacement-time curves at each (T,σ) condition. As mentioned earlier, the fits are only carried out after the finite-size reflections have subsided and the dislocations move in a continuous manner. By way of example, in Fig. 3 we show the fit for the simulation at 630 MPa, which yields a velocity of 244 m s^{-1}. The velocities obtained in this fashion are plotted in Fig. 4 for the four temperatures considered in this study: 100, 200, 300, and 500 K. From here onwards,

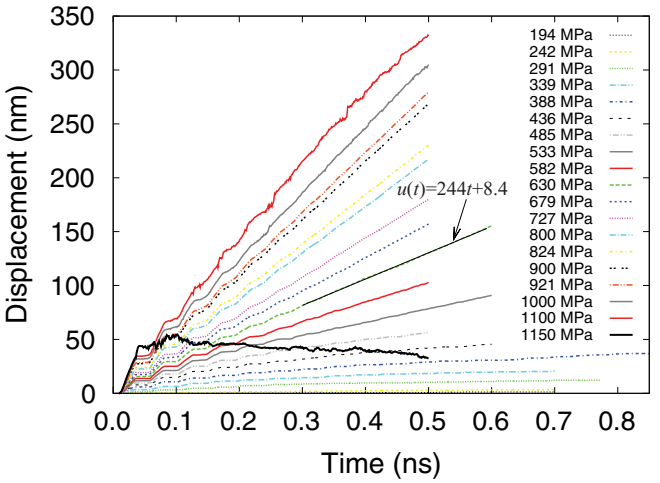

FIG. 3. (Color online) Dislocation displacement vs time at 300 K for all stresses considered here. The curves display an initial serrated behavior, followed by a steady state characterized by smooth glide. A linear fit to the smooth section of the curve for 630 MPa is shown, yielding a velocity of 244 m s^{-1}.

we refer to the applied stress generically as σ, noting that the actual stress that the dislocations suffer after the steady state has been reached typically oscillates at $\approx\pm 10\%$ owing to the the finite-size effects described in Sec. II B.

Two regimes can be visually identified in Fig. 4, more ostensibly at lower temperatures. Initially, at low applied stresses, an exponential regime is clearly recognized, while at higher stresses, the behavior is clearly linear. The dynamic transition is sharp at 100 and 200 K, but becomes considerably more blurred at 300 K and, especially, 500 K. The inset to the figure shows the same data points on a logarithmic scale in an attempt to facilitate the identification of the dynamic transition, which is seen to occur at decreasing stresses with increasing temperature. These transition stresses are denoted by σ^*. Mathematically, σ^* is computed as the inflection stress, i.e., that at which the $v(\sigma)$ function transitions from convex to concave (in other words, when the local derivative of the v-σ

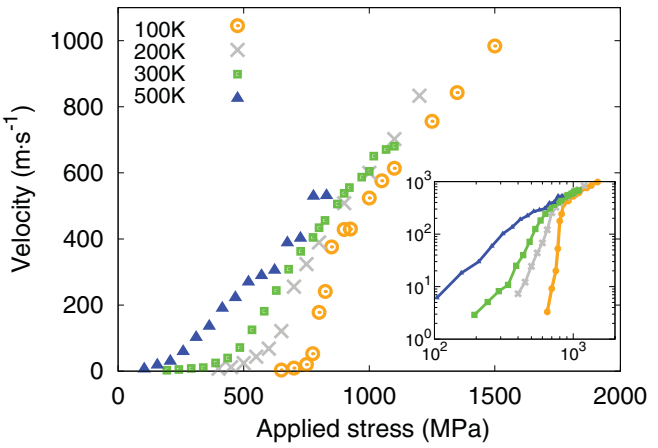

FIG. 4. (Color online) Dislocation velocities against applied stresses for all the temperatures considered here. The inset shows the same data on a logarithmic scale, which allows for a better identification of the dynamic transition.

TABLE I. Calculated values of all temperature-dependent coefficients.

Temperature (K)		100	200	300	500
Threshold stress (MPa)	σ_0	650	400	194	104
Transition stress (MPa)	σ^*	797	770	633	312
Friction coefficient ($\times 10^{-4}$ Pa s)	$\mathcal{B}$	2.7	2.3	2.6	2.9
Transition velocity (m s^{-1})	v^*	419	515	324	167

curve starts to decrease). At 500 K, this occurs over a stress range more than at a specific value, and thus here we have chosen $\sigma^*(500\ \mathrm{K})$ as the first value in that stress range. The values of σ_0 and σ^* are given in Table I and plotted in Fig. 5 as a function of temperature.

The exponential regime corresponds to a thermally activated mechanism of motion governed by KP nucleation, whereas the linear regime is the manifestation of some type of viscous motion. It is unclear if the latter corresponds to the classic phonon drag mechanism, as its onset occurs at stresses $<\sigma_P$, although, due to the displayed linearity, the same theoretical treatment will be applied. In this context, $\sigma^*(T)$ has the meaning of a temperature-dependent transition stress, above which the *free*-energy landscape is flat and the dislocation does not need to overcome any *effective* energy barrier. These transition stresses deserve special attention. The σ^* signal the transition from thermally activated motion to viscous damping at each temperature. Evidently, at 0 K, $\sigma^*(0) \equiv \sigma_P$, but as the temperature increases, the required stress for KP nucleation decreases. As we shall see, it is foreseeable to reach a temperature at which thermally activated KP formation is no longer needed to attain dislocation motion, even at zero stress. This can be qualitatively appreciated in the shape of the curves in Fig. 4, which gradually adopt a more "linearlike" shape as T increases. We shall come back to these issues in Sec. IV.

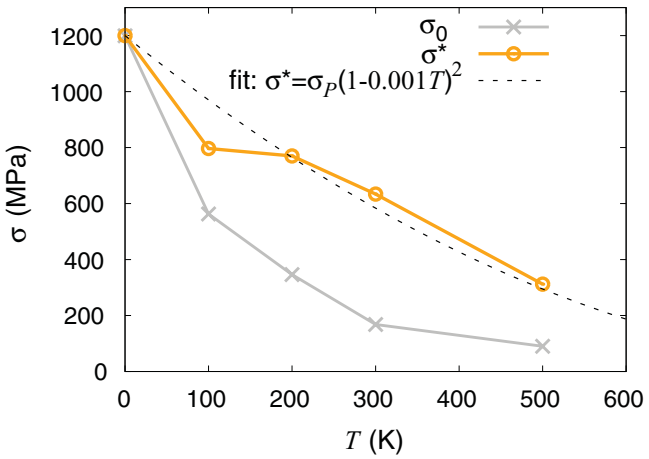

FIG. 5. (Color online) Evolution of the transition and threshold stresses with temperature. Also shown is the fit for σ^* based on the assumed existence of an equivalence between the KP formation enthalpy H and kT. The fit provides a reasonable agreement with the MD data, and predicts a temperature of 1000 K for $\sigma^* = 0$.

B. Mechanism of motion

Next, we describe some aspects of the mechanism of motion for $\sigma < \sigma^*$. We emphasize that this is the stress regime in which the dislocation truly moves by a thermally activated mechanism. Several workers have demonstrated the kink-pair mechanism in 3D dynamic simulations of $\frac{1}{2}\langle 111\rangle$screw dislocation motion for the Mendelev potential,[18,30] and we do not discuss it further here. Rather, we focus on the relationship between KP nucleation and glide plane.

As pointed out earlier, in the conditions where a {112} plane is the MRSS plane, the two {110} planes bordering it at $\pm 30^\circ$ are equally stressed with a RSS factor of $\sqrt{3}/2$. At the same time, the elastic energy of a KP can be shown to be proportional to the kink's height h.[35,36] In the bcc crystal structure, $h^{\{110\}}/h^{\{112\}} = 1/\sqrt{3}$, and for this potential, $\sigma_P{}^{\{110\}} \approx \sigma_P{}^{\{112\}}$. When coupled with the repulsive image forces discussed in Sec. II B, this picture favors alternating jumps between both {110} planes in our simulation setup. Indeed, we have analyzed the dislocation motion at 100 and 500 K at stresses below the corresponding σ^*, and we have confirmed this mechanism. Figure 6 shows the average path of the dislocation core on the [111] plane during a time interval where an equal number of steps on the two bordering planes was observed. The figure clearly shows a serrated profile consistent with kink nucleation on {110} planes.

As a consequence, at low stress and temperature, {112} glide is only *effective*, i.e., the overall glide plane observed from length scales far above the atomistic one is {112}, while it actually occurs by a succession of {110} slip events observable only at the atomic level. For this reason, for σ_P, we use the value of 1200 MPa calculated by Chaussidon *et al.*[30] for {110} planes, since these are the planes where kinks form even if the MRSS plane is of the {112} type. At higher temperatures and stresses, one could expect significant deviations from this alternating slip mechanism as thermal fluctuations smear

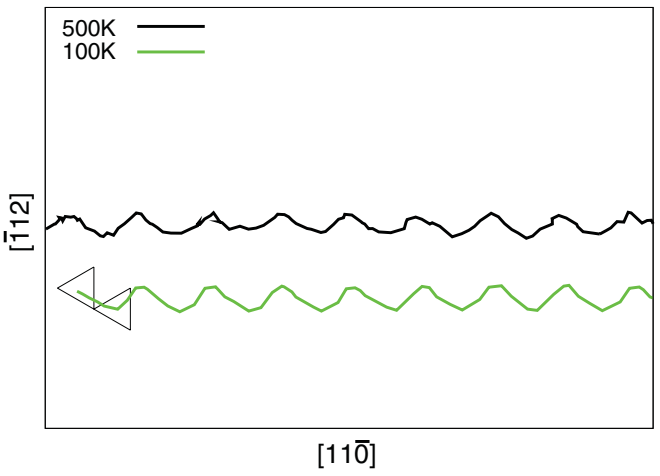

FIG. 6. (Color online) Average trajectory of the dislocation core at 100 and 500 K in the thermally activated motion regime. Two triangles of the $\langle 111\rangle$ zone are shown to scale. The dislocation is clearly seen to move on alternating {110} planes. Not shown are parts of the trajectory where the dislocation concatenated two or more consecutive displacements on the same {110} plane (therefore moving off-plane).

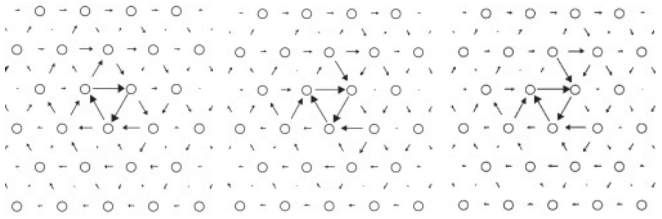

(a) 350K (b) 400K (c) 500K

FIG. 7. Screw dislocation core structure at finite temperature illustrated using differential displacement maps (Ref. 37). The core suffers a transformation from compact to dissociated between 350 and 400 K. Core configurations have been obtained by averaging the atomic positions over 1 ps.

the (repulsive) effect of the traction boundaries. However, in analyzing the dislocation core carefully, we have seen that it undergoes a structural transformation from compact to dissociated between 350 and 400 K, as clearly illustrated in Fig. 7. Dissociated cores are known to have a more limited set of transition pathways compared to compact cores, leading to a mechanism of motion akin to the so-called pencil glide[16] (although they also typically have lower Peierls stresses). Interestingly, however, the analysis at 500 K shown in Fig. 6 resulted in no appreciable differences with respect to that obtained at 100 K.

Some workers have suggested that under certain conditions, slip takes place by KP production on {112} planes.[3,38] If this is interpreted as meaning that KP are created directly on {112} planes, i.e., with height equal to $h^{\{112\}}$, then our observations are in disagreement with that interpretation. However, if the elementary slip step on {112} planes is understood as being composed of two correlated, as opposed to independent, KP events on two {110} planes, then we do not have enough evidence to establish whether that is what our simulations are showing. Detailed time-resolved information, with more resolution than provided in this paper, should help shed light on the issue.

C. Mobility functions

1. Thermally activated regime

In the following, we use the theory of Dorn and Rajnak[35] to extract a functional form for the dislocation velocity as a function of stress and temperature in the thermally activated regime. According to their work, the forward velocity of a dislocation moving by a kink-pair mechanism is

$$v_{th} = h J_k, \tag{1}$$

where, as above, h is the kink height and J_k is the kink-pair nucleation rate. Equation (1) assumes that the kink velocity v_k is large compared to the rate of nucleation. J_k is directly proportional to the available length X for a kink pair to propagate before it annihilates with kinks of opposite sign (kink mean free path):

$$J_k = \frac{\nu_0 X}{s_k} \exp\left[-\frac{F_{\mathrm{KP}}(\sigma)}{kT}\right], \tag{2}$$

where s_k is again the separation between kinks in a KP, ν_0 is an attempt frequency, and F_{KP} is the stress-dependent free energy of a KP. As Dorn and Rajnak noted, at low strain rates, X may be equal to the total dislocation length L, i.e., only one KP exists on the dislocation line at a given time. In such conditions, the frequency with which a nucleated KP glides out of L, i.e., $\nu_a = 2v_k/L$, is much greater than J_k, i.e., $\nu_a \gg J_k$. However, at high strain rates, like those attained during MD simulations, X may be sufficiently small for ν_a and J_k to be comparable. Then,

$$J_k = \frac{\nu_0 X}{s_k} \exp\left[-\frac{F_{\mathrm{KP}}(\sigma)}{kT}\right] = \frac{2v_k}{X},$$

from which

$$X^2 = \frac{2 s_k v_k}{\nu_0} \exp\left[\frac{F_{\mathrm{KP}}(\sigma)}{kT}\right]. \tag{3}$$

By combining Eqs. (1)–(3), we arrive at the general expression for the velocity of a dislocation moving by a thermally activated mechanism,

$$v_{th} = h\sqrt{\frac{2v_k \nu_0}{s_k}} \exp\left[-\frac{F_{\mathrm{KP}}(\sigma)}{2kT}\right]. \tag{4}$$

The kink velocity is assumed to be limited by phonon drag according, e.g., to Liebfried's theory,[39]

$$v_k = \frac{b\sigma}{B_k} = \frac{10}{3}\frac{c_t b^3 \sigma}{kT}, \tag{5}$$

where B_k is a friction coefficient, and c_t is a limiting shear wave velocity. Equation (4) reduces to

$$v_{th} = h\sqrt{\frac{20}{3}\frac{c_t b^3 \nu_0 \sigma}{s_k kT}} \exp\left[-\frac{F_{\mathrm{KP}}(\sigma)}{2kT}\right]. \tag{6}$$

With regard to F_{KP}, experimental studies have shown that the kink-pair entropy S_{KP} is a negligible fraction of the total free energy,[40] and thus it is discarded here. This is substantiated by recent atomistic calculations of the vibrational entropy of finite screw dislocation segments.[41] Therefore, we substitute F_{KP} for the formation enthalpy H_{KP} of a kink pair. Next, instead of using the expressions for H_{KP} derived by Dorn and Rajnak using isotropic linear elasticity, we choose to fit our MD results to the phenomenological expression due to Kocks, Argon, and Ashby,[42]

$$H_{\mathrm{KP}}(\sigma) = H_0\left[1 - \left(\frac{\sigma}{\sigma_n}\right)^p\right]^q, \tag{7}$$

where H_0 is the KP formation enthalpy at zero temperature and stress, and σ_n is a normalizing stress taken to represent the stress at which the KP formation enthalpy vanishes. This stress is typically taken to be the Peierls stress σ_P under static conditions. However, at finite temperature, σ_n must be interpreted as the stress at which the KP free energy of formation vanishes, which, as shown in Sec. III A, is temperature dependent. This is precisely the definition of σ^*, which we thus use as the normalizing stress in Eq. (7). For the adjustable parameters p and q, one can use the values predicted by linear elasticity for a sinusoidal potential, $p = 0.5$ and $q = 1.25$. However, in a periodic box, the activated state becomes distorted by the periodic image interactions (in the

low-stress limit) or by kink spreading (in the limit of stress approaching Peierls threshold). Therefore, we leave p and q as fitting parameters to be obtained from the MD data.

Equations (6) and (7) form a closed functional mobility law for screw dislocations for thermally activated motion. Next, the objective is to devise a global fitting procedure that retains only the stress and temperature dependence, i.e., a universal mobility function that can be used in the entire T and σ range. To this end, we first reduce the explicit stress dependence in Eqs. (6) and (7) for numerical convenience to a nondimensional form described by $s(T) = \sigma/\sigma^*(T)$. Additionally, we condense all the physical parameters in Eq. (6) into a single fitting constant A. The reduced expression is

$$v_{th} = A\sqrt{\frac{s}{T}}\exp\left[-\frac{3772}{T}(1-s^p)^q\right], \tag{8}$$

where we have used $H_0 = 0.65$ eV, which is the value obtained by molecular statics for the potential employed here.[17] This is in reasonable agreement with experimental estimates for H_0 from stress-relaxation measurements in Fe, which range between 0.8 and 1.0 eV.[43–46]

Using Eq. (8) and the transition stresses in Table I, we perform a global least-squares fit to the data in Fig. 4 and obtain values of $A = 3710\,(\pm 146)$ m s^{-1} K$^{1/2}$, $p = 0.51\,(\pm 0.16)$, and $q = 1.07\,(\pm 0.11)$. As Fig. 8 shows, the resulting mobility function provides a very good fit for the velocities corresponding to the thermally activated regime, with the exception of perhaps 500 K. The overall fitting error is approximately 5%. Interestingly, the computed values of p and q almost coincide with those chosen by Naamane *et al.*,[47] who used a thermally activated mobility law which does account for both forward and backward jumps. After rounding down the obtained fitting parameters, the mobility function in numerical form becomes

$$v_{th}(s,T) \approx 3710\sqrt{\frac{s}{T}}\exp\left[-\frac{3772}{T}(1-\sqrt{s})\right].$$

The value of A can be useful to extract parameters related to the prefactor in Eq. (6). For example, one can calculate the value of B_k at different temperatures. In our case, between 100 and 500 K, B_k takes values of the order of 5 to 10×10^{-4} Pa s, which is approximately two to four times larger than the friction coefficient of a rigid screw dislocation, as we shall see.

To fully close the mobility law, one must provide the temperature dependence of σ^* through some suitable analytical law. Following Ngan and Wen,[33] and Domain and Monnet,[13] we assume that there exists an equivalence between the activation energy and the temperature at a constant strain rate. For example, at a strain rate of 1.7×10^{-4} s^{-1}, a ratio of $H/kT \approx 27$ was proposed experimentally.[48] It is unclear what this equivalence is at the specific strain rates attained here, but, following the same argument, one can use the fitted Eq. (7) and assume that

$$T \propto H_{\mathrm{KP}} = H_0\left(1-\sqrt{\frac{\sigma^*}{\sigma_P}}\right),$$

or, in terms of σ^*,

$$\sigma^* = \sigma_P\,(1-CT)^2, \tag{9}$$

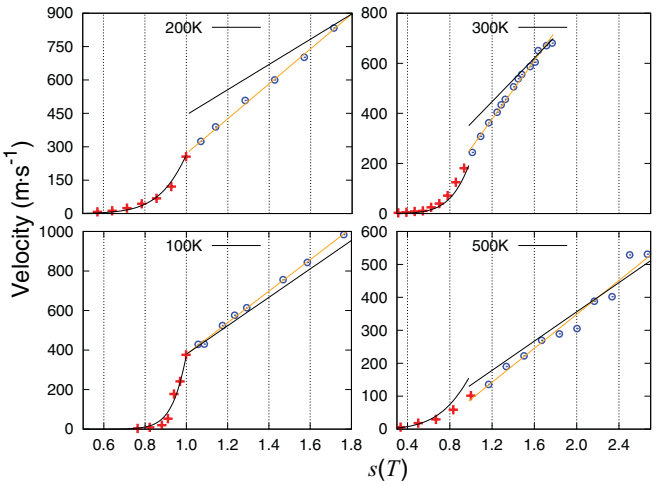

FIG. 8. (Color online) Comparison between the fitted mobility laws and the MD data at each temperature. We note that the mobility is not continuous at σ^*, and that an appropriate "stitching" between the mobilities in each regime must be performed prior to their use in DD simulations. The orange lines represent the individual fits according to Eq. (12).

where C is a proportionality constant. Fitting the σ^*-T data points in Table I to Eq. (9) with $\sigma_P = 1200$ MPa yields $C = 10^{-3}\,(\pm 10^{-4})$ K^{-1}. The fitted Eq. (9) is also shown in Fig. 5. Incidentally, the above expression predicts a value of $\approx$1000 K as the temperature at which the transition stress vanishes. The final mobility function in the thermally activated regime is then

$$\begin{aligned} s &= \frac{\sigma}{1200(1-0.001T)^2} \\ v_{th}(s,T) &= 3710\sqrt{\frac{s}{T}}\exp\left[-\frac{3772}{T}(1-\sqrt{s})\right], \end{aligned} \tag{10}$$

which gives the screw dislocation velocity for each (σ, T) pair.

2. *Linear regime*

At shear stresses above σ^*, the dislocations clearly transition into a linear velocity regime governed by viscous damping. In principle, one could use a universal fitting function of the type

$$v_l(T) = d(s-1) + e, \tag{11}$$

where d and e are also temperature-dependent constants, and the independent variable is scaled to reflect validity only for $\sigma > \sigma^*$. d is inversely proportional to the friction coefficient $\mathcal{B}$ and, in principle, should scale with temperature as $\sim T^{-1}$ [cf. Eq. (5)]. For its part, e should be related to the velocity corresponding to σ^*, i.e., the *transition* velocity v^*. However, because we have no *a priori* information about the temperature dependence of these constants, we first fit each linear mobility data set in Fig. 4 individually using the standard viscous law

$$v_l = \frac{\sigma b}{\mathcal{B}(T)} + v^*(T). \tag{12}$$

In this fashion, we compute $\mathcal{B}$ and v^* for each T to gain insight into their temperature dependence. The results of the fit are shown in Fig. 8 as orange lines. The values

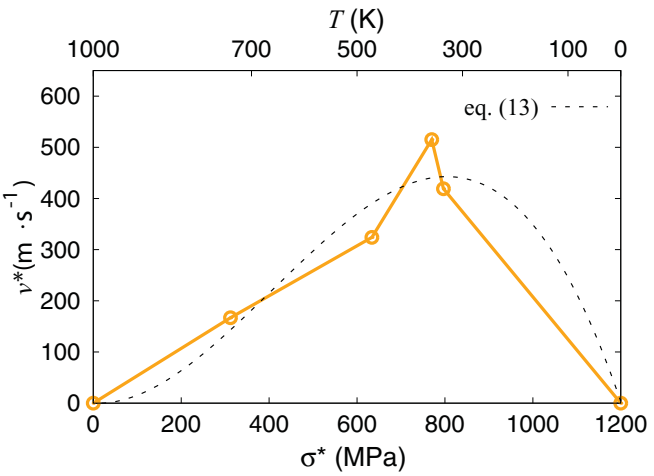

FIG. 9. (Color online) Dependence of the transition velocity v^* with σ^* and T. The temperature axis has been produced from the σ^*-T relationship given in Eq. (9).

for $\mathcal{B}$ and v^* are given in Table I. As the data show, $\mathcal{B}$ displays virtually no temperature dependence, while that of the transition velocities is not clear at first glance. In searching for a suitable temperature dependence for v^*, we note that v^* must be zero both when $\sigma^* = 0$ and when $\sigma^* = \sigma_P$. This is because those are the two instances when there is no longer a need for thermally activated KP nucleation to attain dislocation motion. In terms of temperature, these two limits correspond, respectively, to the temperature at which the activation free energy vanishes [estimated from Eq. (9) at approximately 1000 K], and 0 K. v^* is plotted as a function of σ^* and T in Fig. 9, where the temperature scale follows Eq. (9). To ensure $v^*(\sigma^* = 0) = 0$, we fit the data shown in the figure to a third-degree polynomial of the type

$$v^* = \sigma^*(c_2\sigma^{*2} + c_1\sigma^* + c_0),$$

which results in $c_0 = -4.4 \times 10^{-2}$, $c_1 = 2.2 \times 10^{-3}$, and $c_2 = -1.8 \times 10^{-6}$ (we omit the units of the fitting constants for clarity). The fitted polynomial is also shown in Fig. 9. The dependence with temperature is trivially obtained by substituting $\sigma^* = 1200(1 - 0.001T)^2$ into the fitted polynomial and eliminating the independent term to force $v^* = 0$ at $T = 0$:

$$\begin{aligned} v^*(T) = {} & 6.1T - 2.8 \times 10^{-2}T^2 + 4.9 \times 10^{-5}T^3 \\ & - 4.3 \times 10^{-8}T^4 + 1.9 \times 10^{-11}T^5 \\ & - 3.1 \times 10^{-15}T^6. \end{aligned} \tag{13}$$

By using Eqs. (12) and (13), we can now expand Eq. (11) into a mobility law for the linear regime as

$$\begin{aligned} v_l(s,T) = {} & d(s-1) + 6.1T - 2.8 \times 10^{-2}T^2 + 4.9 \times 10^{-5}T^3 \\ & - 4.3 \times 10^{-8}T^4 + 1.9 \times 10^{-11}T^5 - 3.1 \times 10^{-15}T^6, \end{aligned}$$

where d is related to the *average* friction coefficient $\mathcal{B}' = 2.6 \times 10^{-4}$ Pa s^{-1} (from Table I) via the relation $d = b\sigma^*/\mathcal{B}'$. This relation implicitly introduces a temperature dependence for d by way of $\sigma^*(T)$ from Eq. (9), i.e.,

$$d = \frac{b\sigma_P(1-0.001T^2)}{\mathcal{B}'} \approx 1140 - 2.28T + 1.14 \times 10^{-3}T^2. \tag{14}$$

The final mobility function in the linear regime is, therefore,

$$\begin{aligned} v_l(s,T) = {} & (s-1)(1140 - 2.28T + 1.14 \times 10^{-3}T^2) \\ & + 6.1T - 2.8 \times 10^{-2}T^2 + 4.9 \times 10^{-5}T^3 \\ & - 4.3 \times 10^{-8}T^4 + 1.9 \times 10^{-11}T^5 \\ & - 3.1 \times 10^{-15}T^6, \end{aligned} \tag{15}$$

which gives the velocity in m s^{-1} when T is given in K. The results of this fit are also shown in Fig. 8.

Thus, a closed-form mobility function for $\frac{1}{2}\langle 111\rangle$screw dislocations in α-Fe gliding on {112} planes in the twinning sense as a function of stress and temperature is proposed based on MD simulations:

$$v(s,T) = \begin{cases} 3710\sqrt{\frac{s}{T}}\exp\left[-\frac{3772}{T}(1-\sqrt{s})\right] & \text{for} \quad s \leqslant 1, \\ 1140s - 2.28sT + 1.14 \times 10^{-3}sT^2 - 1140 + 8.4T - 0.03T^2 - 4.9 \times 10^{-5}T^3 \ (\text{m s}^{-1}) \\ \quad + 4.3 \times 10^{-8}T^4 - 1.9 \times 10^{-11}T^5 + 3.1 \times 10^{-15}T^6 \quad \text{for} \quad s > 1, \end{cases} \tag{16}$$

where $s = \frac{\sigma}{1200-2.4T+0.0012T^2}$.

IV. DISCUSSION AND CONCLUSIONS

In this paper, we have carried out simulations of $\frac{1}{2}\langle 111\rangle(1\bar{1}2)$ screw dislocation motion as a function of stress and temperature in order to fit functional mobility laws to be used in mesoscale methods. Below we discuss several aspects related to the validity of our approach and the applicability of the mobility functions proposed.

Let us start by discussing the validity of MD simulations for this task, *vis a vis* the high attendant strain rates. Dislocation motion simulations can be run prescribing the strain rate[13] or, alternatively, the applied stress.[26,30] If one chooses the former, the velocity of the dislocation is also prescribed, and the corresponding stress is extracted as the output of the simulations. Because the strain rates, for dislocations to have a noticeable motion within MD time scales, have to be exceedingly high, it is difficult to argue against the statement that MD strain rates are often excessively above realistic experimental ones. However, if one performs stress-controlled

simulations, it is the velocity that is the output, not the strain rate. Velocities are related to the strain rate through Orowan's equation ($\dot{\varepsilon} = \rho_d v b$, where ρ_d is the dislocation density). However, for a fixed dislocation line length, one can obtain converged mobilities above a certain box size. This means that the measured velocity does not change even if the box dimensions (except the line length) are increased arbitrarily, i.e., ρ_d is decreased arbitrarily. Then, the σ-v relation becomes an upper bound of the mobility, independently of the strain rate.

Next, we discuss the suitability of the fitting functions given in Eq. (16). Equation (8) describes the relation between v and σ and T in the thermally activated regime. The functional form for H_{KP} given by Eq. (7), although phenomenological in nature, is known to provide a good linkage between H_0 and zero as a function of the applied shear stress, and has been widely used in the literature.[19,31,32] The exponents p and q obtained here are in very good agreement with the values predicted by (isotropic) linear elasticity and those used in DD calculations.[19,47] This is an interesting result in light of the fact that α-Fe is a highly anisotropic and nonlinear elastic solid. It is important to emphasize that in Eq. (7), we have used σ^*, rather than σ_P, as the normalizing stress. This is because the σ^* are the limiting stresses after which thermally activated motion is no longer needed at each temperature. Therefore, the transition stresses act as the finite-temperature counterparts of the Peierls stress at 0 K. This, of course, does not change the definition of σ_P, which emanates from the static-energy landscape and is independent of temperature. Simply put, the free-energy barrier decreases (softens) with increasing temperature, thereby necessitating a lower stress to be overcome. Because of this, the definitions of σ^* and σ_P coincide at zero temperature, so that, in a way, the transition stress may be considered a finite-temperature generalization of the concept of Peierls stress.

With regard to the linear regime of motion, there are some considerations to bear in mind. First, we have assumed a polynomial form for the variation of the transition velocity v^* with temperature. This was done purely for numerical convenience, as this form manages to provide a reasonable fit to the data given in Fig. 9. However, even though there is no physical basis behind this choice, we have imposed the temperatures (stresses) at which v^* should vanish, which do have a physical justification. Second, independent linear fits to the MD values at each temperature reveal almost no temperature dependence of the viscous drag coefficient $\mathcal{B}$. This lack of a temperature dependence for $\mathcal{B}$ precludes us from defining this regime as the phonon drag regime. However, we speculate that this could well be a scale-dependent effect, where elastic waves emitted by the dislocation as well as lattice phonons do not have time to fully equilibrate, resulting in a *seemingly* athermal behavior when, in reality, it is just a consequence of small-scale dynamics. In any case, as a word of caution, we do not claim to be realistically capturing the physics of this regime, and this should be kept in mind when using these dislocation mobilities in other higher-level methods.

Next, let us analyze the issues associated with {112} glide. As was stated in Sec. I, slip in bcc materials is known to proceed principally on {110} planes. However, while at low temperatures and stresses, the potential used in this work predicts screw dislocation glide on {110} planes, above room temperature, the effective glide plane is seen to rotate to a {112} configuration.[30] Incidentally, we have shown that above 350 K, the dislocation core loses its compact structure and adopts a more extended structure. Whether this *effective* plane rotation is related to the core transformation is not clear, although, as Fig. 6 shows, the dissociated core configuration is seen to have little or no effect on the glide dynamics at 500 K. Indeed, we have shown that slip proceeds always by way of elementary {110} episodes of KP formation, regardless of what the *effective* glide plane is seen to be. Direct evidence for this mechanism had heretofore been lacking, although, using the nudged elastic band method, Duesbery had shown that the activated state between two equivalent core configurations on a {112} plane was in fact the same as on a {110} plane.[49]

Because of the above arguments, the critical and transition stresses measured here actually pertain to KP formation on {110} planes and can thus be compared directly with other calculations and experimental data associated with {110} slip. To remove the dependence on the quantitative differences between experiments and atomistics regarding the Peierls stress, we compare the temperature dependence of the ratio σ_0/σ_P obtained here with results from several sources in Fig. 10. The calculations by Domain and Monnet[13] and the static results of Wen and Ngan (using a different interatomic potential),[16] normalized to the corresponding Peierls stress, are included in the figure. In addition, the experimental data from Kuramoto *et al.*[5] and Brunner and Diehl[6] are also shown. Both of these experiments were carried out under conditions that favor glide on {110} planes at strain rates $< 10^{-4}$ s^{-1}.

As the figure demonstrates, despite the differences in the attendant strain rates, the agreement for $T < 300$ K between our data and both experimental and atomistic calculations is excellent. However, at higher temperatures, the MD calculations deviate from the static values in that they appear to saturate or decline more slowly to their zero value. Future

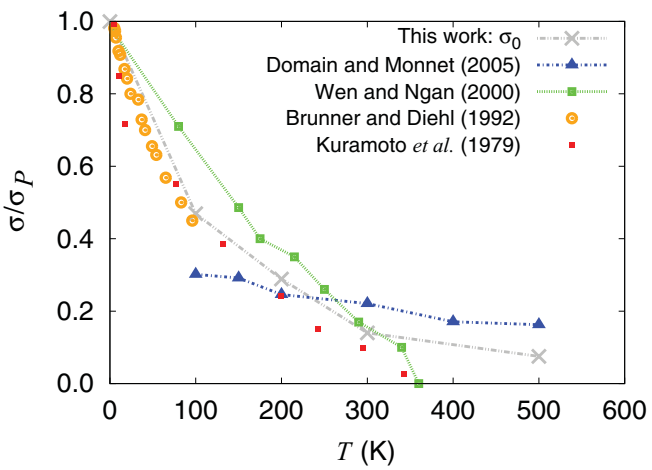

FIG. 10. (Color online) Comparison of the normalized threshold stress obtained in this work to atomistic results (Refs. 13 and 16) and the experimental values of the flow stress in pure single Fe crystals measured by Kuramoto *et al.* (Ref. 5) and Brunner and Diehl (Ref. 6). The normalization factors for the experimental data were 363 (Ref. 47) and 380 MPa, respectively.

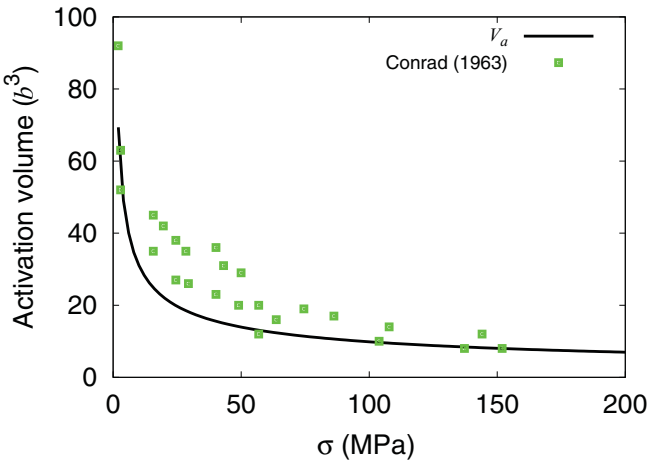

FIG. 11. (Color online) Comparison between the theoretical activation volume, as given by Eq. (17), and the experimental data for Fe by Conrad (Ref. 50).

studies will determine the temperature at which the threshold stress vanishes for the Mendelev potential.

Further, as noted by Dorn and Rajnak,[35] the most reliable verification of the Peierls mechanism is to compare experimentally and theoretically deduced activation volumes. From Eq. (7), assuming $p = \frac{1}{2}$ and $q = 1$, the expression for the activation volume can be obtained as $V_a = \partial H/\partial\sigma$:

$$V_a = \frac{\partial H}{\partial \sigma} = \frac{H_0}{2\sqrt{\sigma_P}} \frac{1}{\sqrt{\sigma}}, \tag{17}$$

which is compared in Fig. 11 with the data for bcc Fe compiled by Conrad.[50] As is the case in other theoretical studies, V_a underestimates the experimental data in the $0 < \sigma < 100$ MPa interval. This has been attributed to a strong dislocation density dependence with stress in that range. For $\sigma = \sigma_P$, the theoretical activation volume takes a value of 2.8 b^3.

As a final remark, we emphasize that the ultimate objective of works such as the present one is to generate mobility laws that can be elevated to higher temporal and spatial scales by being integrated into models of higher statistical level, e.g., dislocation dynamics, phase field, etc. In this sense, we note that our work, which provides mobilities for a given slip system, is only one step in such a direction, and that more calculations on other slip systems, perhaps using other interatomic models, must be carried out before a full mobility law can be produced. In any case, our simulations provide nonlinear laws that represent an improvement over uniform, character-independent variants (known as "BCC0") used in several studies.[51] Other workers have used nonlinear expressions similar to Eq. (6) that are typically fitted to experimental data or molecular statics calculations,[19,20,47] i.e., not obtained in a self-consistent fashion as in this paper. Additionally, a unified mobility function, apt for use in DD, must be continuous and differentiable in the entire stress and temperature ranges. Thus, the numerical usefulness of Eq. (16) for dislocation dynamics calculations hinges on an appropriate "stitching" of the thermal and linear mobilities presented here. This can be achieved using suitable splines or via harmonic averaging.[52] The bivariate polynomial form of the linear velocity regime, which appears as a consequence of the temperature dependence of σ^* and v^*, may be challenging to implement, and suitable simplifications may be in order. However, all of these issues belong to the realm of functional analysis and they are not elaborated on further. With regard to the range of applicability of Eq. (16), the very definition of s imposes a limit of $T = 1000$ K for our mobility function. Evidently we stand by our explored temperature interval of $100 < T < 500$ K, but it is unclear if the functions supplied here are valid beyond it. It is important to emphasize that v_l in Eq. (16) is only meaningful for $s > 1$.

ACKNOWLEDGMENTS

We are greatly indebted to Professor D. Farkas for enabling the use of SystemX at Virginia Tech. We also thank Dr. V. Bulatov for critically reviewing the manuscript and providing many useful suggestions. Productive discussions with Dr. S. Dudarev, Dr. A. Caro, and Prof. G. Taylor are also gratefully acknowledged. This work was performed under the auspices of the US Department of Energy by Lawrence Livermore National Laboratory under Contract No. DE-AC52-07NA27344. We specifically acknowledge support from the Laboratory Directed Research and Development Program under Project No. 09-SI-003. This work was partially funded by the RCUK Energy Programme under Grant No. EP/I501045 and the European Communities under the Contract of Association between EURATOM and CCFE. The views and opinions expressed herein do not necessarily reflect those of the European Commission.

*marian1@llnl.gov

[1]R. R. Kossowsky and N. Brown, Acta Metall. **14**, 131 (1966).
[2]W. Wasserbäch, Philos. Mag. A **53**, 335 (1986).
[3]D. Brunner and J. Diehl, Phys. Status Solidi A **124**, 155 (1991).
[4]T. Suzuki, H. Koizumi, and H. O. K. Kirchner, Acta Metall. Mater. **43**, 2177 (1995).
[5]E. Kuramoto, Y. Aono, and K. Kitajima, Philos. Mag. A **39**, 717 (1979).
[6]D. Brunner and J. Diehl, Z. Metallkd. **83**, 828 (1992).
[7]T. J. Balk and K. J. Hemker, Philos. Mag. A **81**, 1507 (2001).
[8]M. J. Mills, N. L. Baluc, and P. M. Sarosi, Microsc. Res. Tech. **69**, 317 (2006).
[9]D. Caillard, Acta Mater. **58**, 3493 (2010).
[10]R. Chang, Philos. Mag. **16**, 1021 (1967).
[11]P. C. Gehlen, J. Appl. Phys. **41**, 5165 (1970).
[12]T. Harry and D. J. Bacon, Acta Mater. **50**, 195 (2002).
[13]C. Domain and G. Monnet, Phys. Rev. Lett. **95**, 215506 (2005).
[14]L. Ventelon and F. Willaime, J. Comput. Aided Mater. Des. **14**, 85 (2007).
[15]M. S. Duesbery, Acta Metall. **31**, 1747 (1983).

[16]M. Wen and A. H. W. Ngan, Acta Mater. **48**, 4255 (2000).
[17]L. Ventelon, F. Willaime, and P. Leyronnas, J. Nucl. Mater. **386-388**, 26 (2009).
[18]P. A. Gordon, T. Neeraj, Y. Li, and J. Li, Model. Simulat. Mater. Sci. Eng. **18**, 085008 (2010).
[19]M. Tang, L. P. Kubin, and G. R. Canova, Acta Mater. **46**, 3221 (1998).
[20]J. Chaussidon, C. Robertson, D. Rodney, and M. Fivel, Acta Mater. **56**, 5466 (2008).
[21]W. Cai and V. V. Bulatov, Mater. Sci. Eng. A **387-389**, 277 (2004).
[22]*Handbook of Materials Modeling*, edited by S. Yip (Springer, The Netherlands, 2005).
[23]V. V. Bulatov and W. Cai, *Computer Simulations of Dislocations* (Oxford University Press, Oxford, 2006).
[24]J. Chang, W. Cai, V. V. Bulatov, and S. Yip, Mater. Sci. Eng. A **309-310**, 160 (2001).
[25]J. Marian and A. Caro, Phys. Rev. B **74**, 024113 (2006).
[26]J. Marian, W. Cai, and V. V. Bulatov, Nature Mater. **3**, 158 (2004).
[27]S. J. Plimpton, J. Comp. Phys. **117**, 1 (1995).
[28]M. I. Mendelev, S. Han, D. J. Srolovitz, G. J. Ackland, D. Y. Sun, and M. Asta, Philos. Mag. **83**, 3977 (2003).
[29]S. L. Frederiksen and K. W. Jacobsen, Philos. Mag. **83**, 365 (2003).
[30]J. Chaussidon, M. Fivel, and D. Rodney, Acta Mater. **54**, 3407 (2006).
[31]D. Rodney and L. Proville, Phys. Rev. B **79**, 094108 (2009).
[32]G. Monnet, C. Domain, S. Queyreau, S. Naamane, and B. Devincre, J. Nucl. Mater. **394**, 174 (2009).
[33]A. H. W. Ngan and M. Wen, Comput. Mater. Sci. **23**, 139 (2002).
[34]T. C. T. Ting and D. M. Barnett, Int. J. Solids Struct. **30**, 313 (1993).
[35]J. E. Dorn and S. Rajnak, Trans. Metall. Soc. AIME **230**, 1052 (1964).
[36]H. Koizumi, H. O. K. Kirchner, and T. Suzuki, Acta Metall. Mater. **41**, 3483 (1993).
[37]V. Vitek, Cryst. Latt. Def. **5**, 1 (1974).
[38]A. Seeger, Zeitschrift für Metallkunde **93**, 760 (2002).
[39]G. Liebfried, Z. Phys. **127**, 344 (1950).
[40]W. A. Spitzig and A. S. Keh, Acta Metall. **18**, 1021 (1970).
[41]P. C. Schuck, J. Marian, J. B. Adams, and B. Sadigh, Philos. Mag. **89**, 2861 (2009).
[42]U. K. Kocks, A. S. Argon, and M. F. Asby, Prog. Mater. Sci. **19**, 1 (1975).
[43]W. A. Spitzig and A. S. Keh, Acta Metall. **18**, 611 (1970).
[44]S. Takeuchi and K. Maeda, Acta Metall. **25**, 1485 (1977).
[45]A. Seeger, Mater. Sci. Eng. A **319-321**, 254 (2001).
[46]A. Seeger and W. Wasserbäch, Phys. Status Solidi A **189**, 27 (2002).
[47]S. Naamane, G. Monnet, and B. Devincre, Int. J. Plasticity **26**, 84 (2010).
[48]Y. Aono, E. Kuramoto, and K. Kitajima, in *Dislocation Dynamics and Plasticity*, Springer Series in Materials Science Vol. 12 (Springer, Berlin, 1991), p. 94.
[49]M. S. Duesbery (unpublished).
[50]H. Conrad, Philosophical Magazine **5**(55), 745 (1960).
[51]A. Arsenlis and M. Tang, Model. Simulat. Mater. Sci. Eng. **11**, 251 (2003).
[52]N. Barton, J. V. Bernier, R. Becker, A. Arsenlis, R. Cavallo, J. Marian, M. Rhee, H.-S. Park, B. A. Remington, and R. T. Olson, J. Appl. Phys. **109**, 073501 (2011).